El Niño–Related Summer Precipitation Anomalies in Southeast Asia Modulated by the Atlantic Multidecadal Oscillation

YI FAN AND KE FAN

Nansen-Zhu International Research Centre, Institute of Atmospheric Physics, Chinese Academy of Sciences, and University of Chinese Academy of Sciences, Beijing, China

XIUHUA ZHU

Max Planck Institute for Meteorology, and Center for Earth System Research and Sustainability, Meteorological Institute, University of Hamburg, Hamburg, Germany

KLAUS FRAEDRICH

Max Planck Institute for Meteorology, Hamburg, Germany

(Manuscript received 17 January 2019, in final form 15 August 2019)

ABSTRACT

How the Atlantic multidecadal oscillation (AMO) affects El Niño–related signals in Southeast Asia is investigated in this study on a subseasonal scale. Based on observational and reanalysis data, as well as numerical model simulations, El Niño–related precipitation anomalies are analyzed for AMO positive and negative phases, which reveals a time-dependent modulation of the AMO. 1) In May–June, the AMO influences the precipitation in southern China (SC) and the Indochina peninsula (ICP) by modulating the El Niño–related air–sea interaction over the western North Pacific (WNP). During negative AMO phases, cold sea surface temperature anomalies (SSTAs) over the WNP favor the maintaining of the WNP anomalous anticyclone (WNPAC). The associated southerly (westerly) anomalies on the northwest (southwest) flank of the WNPAC enhance (reduce) the climatological moisture transport to SC (the ICP) and result in wetter (drier) than normal conditions. In contrast, during positive AMO phases, weak SSTAs over the WNP lead to limited influence of El Niño on precipitation in Southeast Asia. 2) In July–August, the teleconnection impact from the North Atlantic is more manifest than that in May–June. During positive AMO phases, the warmer than normal North Atlantic favors anomalous wave trains, which propagate along the ''great circle route'' and result in positive pressure anomalies over SC, consequently suppressing precipitation in SC and the ICP. During negative AMO phases, the anomalous wave trains tend to propagate eastward from Europe to Northeast Asia along the summer Asian jet, exerting limited influence on Southeast Asia.

1. Introduction

Southern China (SC) and the Indochina peninsula (ICP) are among the most densely populated areas in the world, and they are vulnerable to hydroclimatic extremes such as floods and droughts. The interannual variability of precipitation in SC and the ICP is greatly affected by ENSO (Huang and Wu 1989; Dai and Wigley 2000; Chen et al. 2014; Zhang et al. 2015; Ge et al. 2017; Lin et al. 2018). A typical ENSO event (for both El Niño and La Niña) matures in winter and decays in the following spring and summer. During the mature phase of El Niño, the local surface cooling over the western tropical Pacific and a warming central Pacific induce an anomalous anticyclone over the western North Pacific (WNPAC) (Wang et al. 2000; T. Li et al. 2017). The WNPAC, influencing the climate over both SC and the ICP, persists from the El Niño maturing winter to its decay in summer, which is maintained by the following factors: the local wind–evaporation–sea surface temperature (SST) feedback (Wang et al. 2000), the combination mode produced by interactions

Supplemental information related to this paper is available at the Journals Online website: https://doi.org/10.1175/JCLI-D-19-0049.s1.

Corresponding author: Prof. Ke Fan, fanke@mail.iap.ac.cn

DOI: 10.1175/JCLI-D-19-0049.1

between the El Niño and the annual cycle (Stuecker et al. 2015; Zhang et al. 2016), the basinwide warming of the Indian Ocean (Xie et al. 2009), and anomalous moist enthalpy advection (Wu et al. 2017). Normally, in the summer of an El Niño decaying year, flood (drought) occurs in SC (the ICP), due to enhanced (reduced) water vapor transport associated with wind anomalies on the west flank of the WNPAC (Zhang et al. 1999; Zhang and Sumi 2002; Lim and Kim 2007; Nguyen et al. 2007; Zhang et al. 2017). However, recent studies have indicated that the correlation between El Niño and the precipitation anomalies in SC may not be stable (Hu and Feng 2012; Wang et al. 2012; Goly and Teegavarapu 2014; Kayano and Capistrano 2014; Chen et al. 2018; C. Li et al. 2017), which could be influenced by midlatitude circulations. For instance, C. Li et al. (2017) suggested that the anomalous midlatitude wave activity was responsible for the drought in SC in August during the El Niño decaying phase in 2016 (which was not the case for the catastrophic flood during the El Niño decaying phase in 1998). Chen et al. (2018) pointed out that the tropical Pacific and Atlantic SSTs jointly led to the unusual drought in SC in the late summer of 2016.

The Atlantic multidecadal oscillation (AMO), a 60–80-yr oscillation of the SST anomaly (SSTA) in the Atlantic Ocean, has been considered as an important pacemaker for the North Hemisphere climate (Kerr 2000). Previous studies indicate that the AMO shows significant impacts on ENSO and its influences on regional climate (Zhang and Delworth 2005, 2007; Li and Bates 2007; Y. Wang et al. 2009; Luo et al. 2011; Geng et al. 2017; Hao and He 2017). First, the AMO induces an anomalous Walker circulation between the tropical Atlantic and the central Pacific (Kucharski et al. 2016). The corresponding surface wind anomalies over the equatorial Pacific are argued to disturb the thermocline based on the Sverdrup balance, and to further impact ENSO variability via modulating the thermocline feedback due to the changed oceanic vertical stratification (Dong et al. 2006; Lu et al. 2008). Second, a warmer than normal North Atlantic during positive AMO phases generates atmospheric responses to the North Pacific, and further leads to warm SSTAs over the western tropical Pacific via a series of air–sea interactions (Sun et al. 2017). Third, the AMO can modulate mid- to high-latitude wave activities, leading to circulation anomalies over East Asia and modifying the ENSO–monsoon relationship (Li et al. 2008; Zhu et al. 2011; Luo et al. 2011; Geng et al. 2017, 2018; Fan et al. 2018).

On one hand, El Niño directly impacts precipitation in SC and the ICP by exerting its influence on the WNPAC. In the meantime, it is under the modulation of the AMO. Considering the essential role of El Niño in climate prediction and risk prevention in Asia, it is of great importance to further investigate how the AMO modulates El Niño–related precipitation anomalies in SC and the ICP.

Previous studies addressing El Niño–related precipitation anomalies have mostly been carried out using seasonal mean data. Recently, subseasonal variability is gaining increasing research interest (B. Wang et al. 2009; Yun et al. 2010; Gill et al. 2015; Jung and Kirtman 2016; Xing et al. 2017). Gill et al. (2015) indicated that the correlation between ENSO and Indian precipitation changes with the monsoonal progression through early (June), middle (July and August), and late summer (September). B. Wang et al. (2009) pointed out that the climate over East Asia in early summer (May and June) shows significant differences compared to those in late summer (July and August). It has also been suggested that only an extreme El Niño will lead to wet anomalies in SC throughout the entire summer, while a normal El Niño will induce wet anomalies during early summer but dry anomalies during late summer (Zhang et al. 1999; Ding and Hu 2003; B. Wang et al. 2009; C. Li et al. 2017). Accordingly, the current study divides summer into early summer [May–June (MJ)] and late summer [July–August (JA)] to separately investigate the variations in precipitation.

The paper is structured as follows: Datasets and methods are briefly described in section 2. Evolutions of the El Niño–related SSTAs during different AMO phases are outlined in section 3a. AMO modulating El Niño–related precipitation anomalies in MJ and JA are investigated in sections 3b and 3c, respectively. Further evaluation of model simulation results is presented in section 3d. A summary and discussion of the study is provided in section 4.

2. Datasets and methods

a. Datasets

In this study, the annual-mean AMO index from 1856 to 2017, which was computed from the area-weighted average over the North Atlantic (0°–70°N), is derived from https://www.esrl.noaa.gov/psd/data/timeseries/AMO (Enfield et al. 2001). The circulation and moisture data are from the Twentieth Century Reanalysis V2c dataset (Compo et al. 2006) covering the period of 1850–2014. The SST data are from the NOAA ERSST v4 dataset, with coverage from 1854 to 2014 (B. Huang et al. 2015). Both these datasets have a resolution of 2° × 2° and are available at http://www.esrl.noaa.gov/psd/. The CRU TS4.01 monthly precipitation dataset from 1901 to 2016, with a horizontal resolution of 0.5° × 0.5°

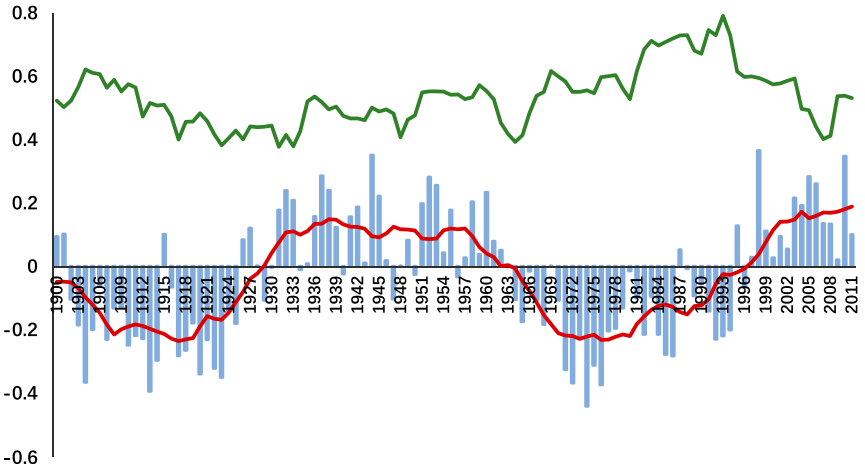

FIG. 1. Time series of AMO (red solid line) and Niño-3.4 (green solid line) indices subject to a 13-yr running mean and standard deviation, respectively (1900–2011). Normalized yearly AMO indices are displayed as blue bars.

(http://data.ceda.ac.uk/badc/cru/data/cru_ts/cru_ts_4.01/data/), is used to investigate the precipitation anomalies over SC and the ICP. In addition, an observation-station-based Chinese (CN05.1) gridded precipitation dataset and the Global Precipitation Climatology Centre (GPCC) monthly precipitation dataset are also employed to verify the precipitation anomalies. The CN05.1 precipitation data are released by the National Climate Center of China, with a resolution of 0.5° × 0.5°, covering the period of 1961–2014 (Wu and Gao 2013). The GPCC monthly precipitation dataset has a resolution of 1° × 1° and covers the period of 1901–2013 (https://www.esrl.noaa.gov/psd/data/gridded/data.gpcc.html). The model simulation data are from the historical simulation (1901–2005) of GFDL CM3 in phase 5 of the Coupled Model Intercomparison Project (CMIP5; Taylor et al. 2012) provided by the NOAA Geophysical Fluid Dynamics Laboratory. Previous studies have demonstrated that GFDL CM3 can reproduce the annual monsoon variations in SC reasonably well (Wang et al. 2013; Fan et al. 2018). Moreover, GFDL CM3 can capture the spatial pattern features of ENSO and the AMO (Griffies et al. 2011; Ruiz-Barradas et al. 2013; Kavvada et al. 2013; Cai et al. 2014). Therefore, we employ the SSTs, circulation, and precipitation outputs of the GFDL CM3 historical simulations in the model evaluation (section 3d). Considering the potentially large spread of model ensembles at longer time scales, five runs of the GFDL CM3 model are evaluated; the runs determine the r1i1p1 member for the following investigations, which shows the most reasonable simulation of the AMO modulated precipitation anomalies (ensemble: r1i1p1; more details at https://esgf-node.llnl.gov/search/cmip5/).

b. Methods

The horizontal anomalous large-scale wave activity flux, according to Takaya and Nakamura (2001), is

$$\mathbf{W} = \frac{1}{2|\overline{\mathbf{u}}|}\begin{bmatrix} \overline{u}(\psi_x'^2 - \psi'\psi'_{xx}) + \overline{v}(\psi'_x\psi'_y - \psi'\psi'_{xy}) \\ \overline{u}(\psi'_x\psi'_y - \psi'\psi'_{xy}) + \overline{v}(\psi_y'^2 - \psi'\psi'_{yy}) \end{bmatrix},$$

where overbars and primes denote mean states and deviations from the mean states, respectively; the subscripts x and y represent zonal and meridional gradients, respectively; $\mathbf{u} = (u, v)$ denotes the horizontal wind velocity components; and ψ' represents the eddy streamfunction.

The AMO is a mode of natural variability occurring in the Atlantic Ocean and has its principal expression in the SST field. The AMO is identified as a coherent pattern of variability in basinwide North Atlantic SSTs with a periodicity of 60–80 years. As shown in Fig. 1, periods with a positive (negative) 13-yr running average AMO index are defined as positive (negative) phases of the AMO. Based on this criterion, two negative AMO periods (1901–29 and 1964–94) and two positive AMO periods (1930–63 and 1995–2014) are identified. The Niño-3.4 index is calculated through the monthly mean of the SSTAs over the Niño-3.4 region (5°S–5°N, 170°–120°W). An El Niño event is identified when the linearly detrended normalized winter (seasonal mean of December, January, and February) Niño-3.4 index is greater than 0.5 from 1901 to 2014. The years with El

TABLE 1. The El Niño events, characterized by the Niño-3.4 indices being greater than 0.5, during positive phases of the AMO (+AMO; i.e., 1930–63 and 1995–2014) and negative phases of the AMO (−AMO; i.e., 1901–29 and 1964–94).

	+AMO	−AMO
El Niño	1931, 1940, 1941, 1942, 1946, 1958, 1995, 1998, 2003, 2005, 2007, 2010	1903, 1905, 1906, 1912, 1914, 1915, 1919, 1920, 1924, 1926, 1964, 1966, 1969, 1973, 1983, 1987, 1988, 1992

Niño under different phases of the AMO are listed in Table 1. Composites of El Niño events during positive phases of the AMO (+AMO) represent the combined effect of El Niño and +AMO (+AMO/EL Niño), and composites of El Niño events during negative phases of the AMO (−AMO) represent the combined effects of El Niño and −AMO (−AMO/El Niño). The basic climatological period for composite anomalies is from 1901 to 2014. In the following investigation, the SC area (20°–30°N, 110°–122°E) and the ICP area (8°–24°N, 90°–110°E) are denoted as Southeast Asia. Wet (dry) anomalies are identified by positive (negative) precipitation anomalies passing the Student's t test at the 95% confidence level. For reanalysis, over the Tibetan Plateau, the fields are masked at layers lower than 850 hPa by the boundary data obtained from the Institute of Geographic Sciences and Natural Resources Research (Zhang et al. 2002).

Following B. Wang et al. (2009), the current study divides summer into early summer (MJ) and late summer (JA) to investigate the precipitation variations separately. As shown in Fig. 2, the climatological settings of circulation and precipitation over SC and the ICP in MJ and JA are different. In MJ, southwesterlies and westerlies prevail over SC and the ICP, respectively, and the monsoon trough is located over the South China Sea (Fig. 2a). In JA, the western North Pacific subtropical high marches to the north, inducing an eastward shifting monsoon trough, which controls both the South China Sea and the Philippine Sea (Fig. 2b). The monsoon precipitation zone expands to both the north and west, covering a larger area in JA (Fig. 2b) compared to MJ (Fig. 2a). Hence, there is also a climatological basis for dividing summer into MJ and JA in the following investigation. Additionally, in this study, the two-month periods of January and February and of March and April are referred to as JF and MA, respectively.

3. Results

a. *The evolution of El Niño–related SSTAs during different AMO phases*

The AMO modulates the El Niño–related summer SSTAs by influencing the ENSO variability and the western North Pacific SSTs. Previous studies have illustrated that the El Niño variability is stronger (weaker) during negative (positive) phases of the AMO (Dong et al. 2006; Goswami et al. 2006; Lu et al. 2006; Lu et al. 2008). As shown in Fig. 1, the AMO and ENSO

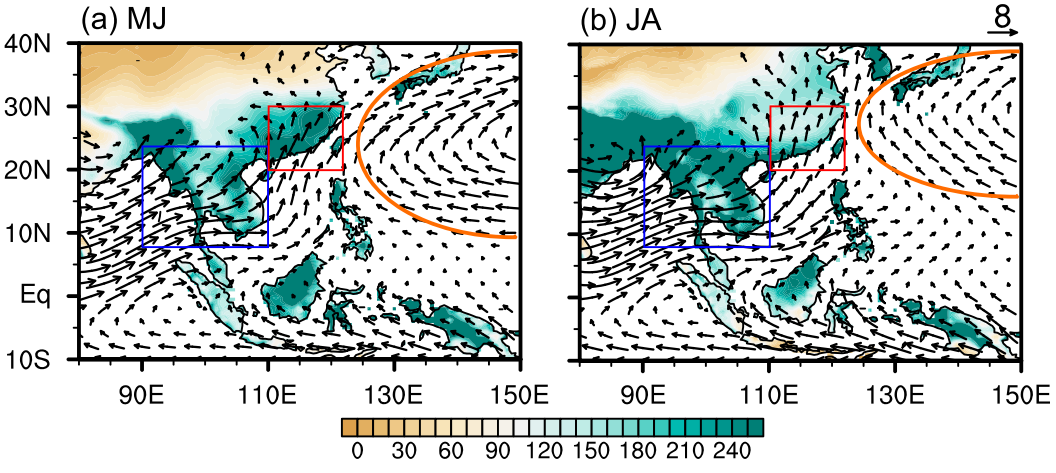

FIG. 2. Climatological mean precipitation derived from the CRU TS4.01 dataset (shading; mm month^{-1}) and the wind field at 850 hPa (vectors; m s^{-1}) in (a) MJ and (b) JA during 1901–2014. The orange curve indicates the position of the western North Pacific subtropical high. The red rectangle marks the SC region (20°–30°N, 110°–122°E), and the blue rectangle marks the ICP region (8°–24°N, 90°–110°E).

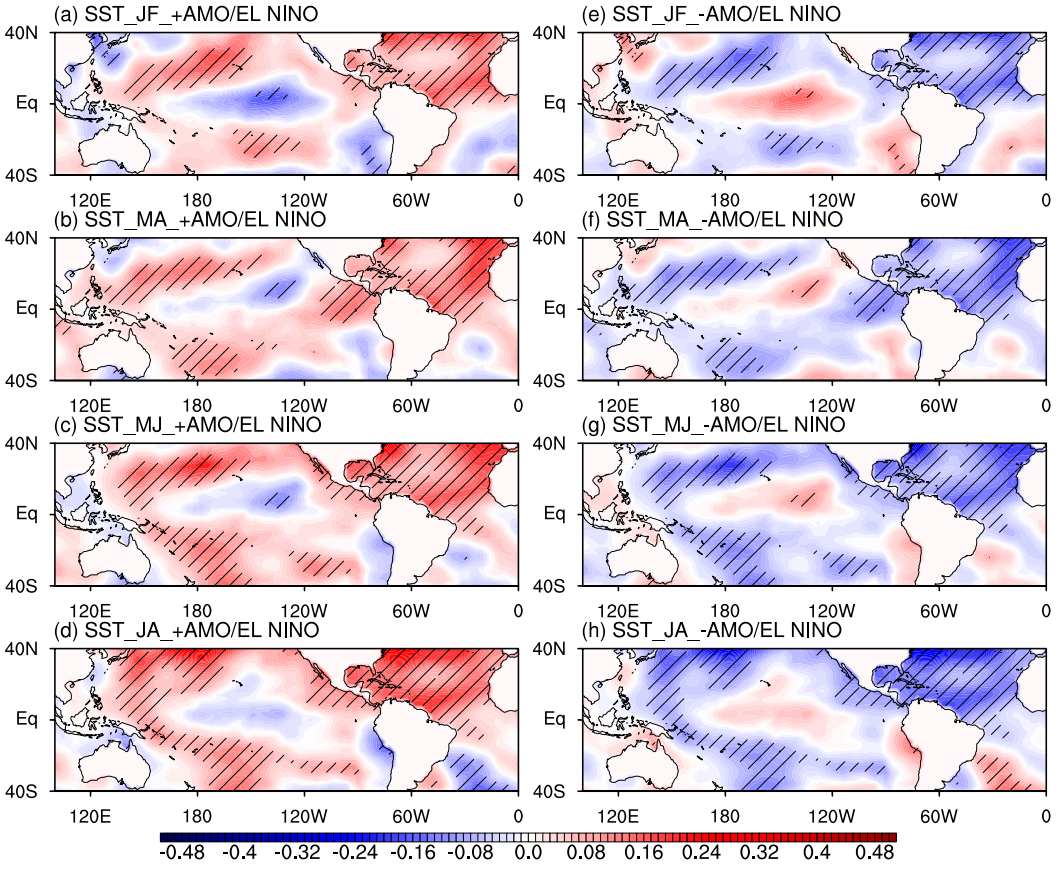

FIG. 3. SST composites of (left) positive AMO phases minus the climatological state and (right) negative AMO phases minus the climatological state during 1901–2014 in (a),(e) JF, (b),(f) MA, (c),(g) MJ, and (d),(h) JA (K). The hatched shading shows statistical significance at the 90% confidence level according to the Student's *t* test.

variability are negatively correlated with their correlation coefficient of −0.30. Moreover, the western Pacific is warmer (colder) than normal during positive (negative) phases of the AMO from JF to JA (Fig. 3). Consequently, the influences of the AMO on the western Pacific SSTs and tropical eastern Pacific, as a long-term period background, produce important impacts on the evolution of the El Niño–related anomalous SST pattern.

Normally, during the mature phase of a typical El Niño event, the central and eastern Pacific (western tropical Pacific) are covered by warm (cold) anomalies (Fig. 4a). This spatial feature persists from JF to MA (Figs. 4a,b) and disappears in JA (Fig. 4d) after a weakening phase in MJ (Fig. 4c). During positive phases of the AMO, since the western North Pacific is warmer (Figs. 3a–d) and El Niño is weaker than normal (Fig. 1), the El Niño–related cold SSTA pattern in the western Pacific weakens earlier: cold SSTAs in the western Pacific only persist from JF to MA (Figs. 4e–f) and almost disappear in MJ (Fig. 4g). By contrast, during negative phases of the AMO, with a colder than normal western North Pacific background (Figs. 3e–h) and a stronger than normal El Niño (Fig. 1), the El Niño–induced cold SSTA pattern in the western North Pacific (Figs. 4i–l) decays more slowly than normal (Figs. 4a–d): the cold (warm) anomaly in the western (eastern) Pacific that persists from JF to MA (Figs. 4i,j) is still visible in MJ (Fig. 4k), and then it weakens in JA (Fig. 4l). Moreover, in JA, the El Niño–related SSTAs are generally weak in the tropical Pacific, in contrast to the strong AMO-related SSTAs in the North Atlantic (Figs. 4h,l), which shows warm (cold) anomalies during positive (negative) AMO phases.

From the above analysis, two essential conclusions can be stated. 1) In MJ, because the El Niño–related SSTA pattern lasts longer during negative phases of the AMO than during positive phases, the cold (warm) anomalies over the western (eastern) Pacific disappear during positive AMO phases (Fig. 4g), whereas they are still significant during AMO negative phases (Fig. 4k). 2) In JA, the SSTAs weaken in the tropical Pacific along

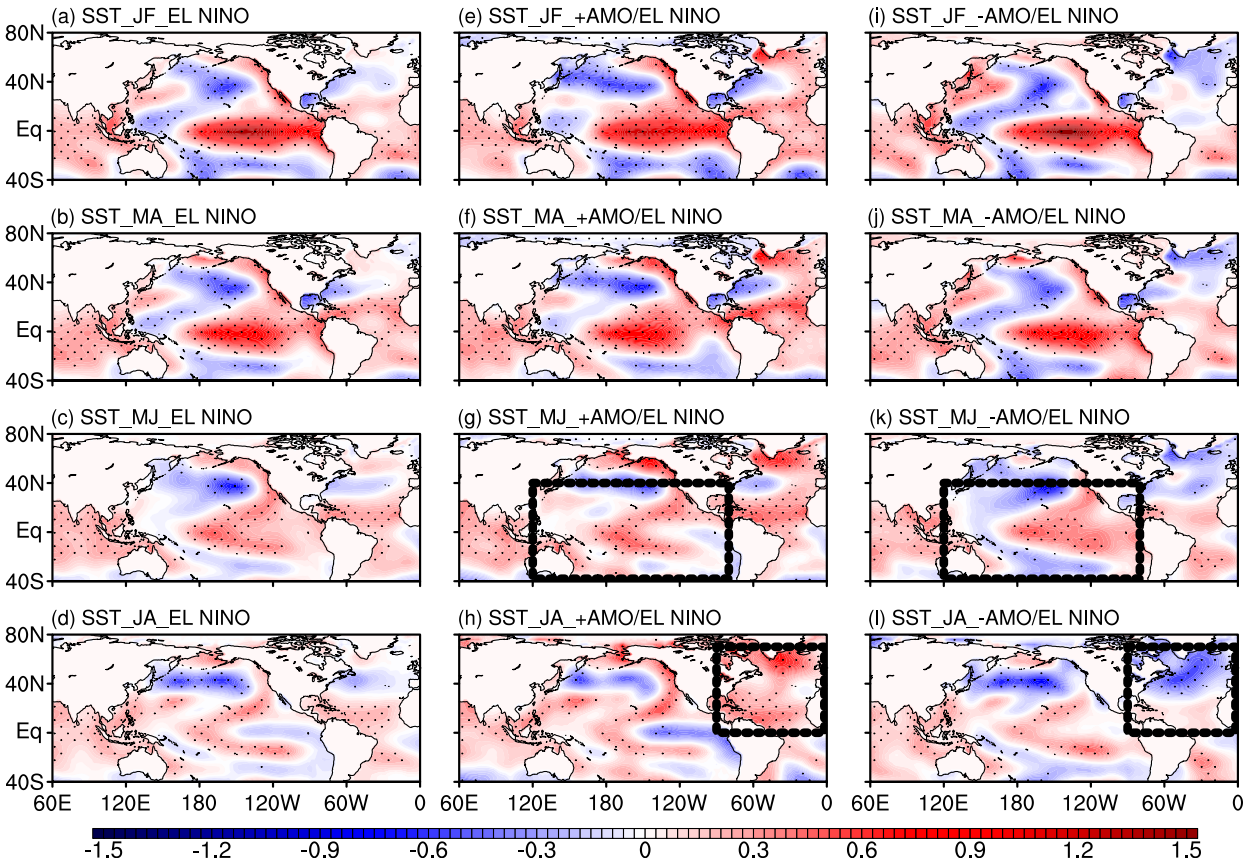

FIG. 4. SST composites of El Niño events (K) in (a),(e),(i) JF, (b),(f),(j) MA, (c),(g),(k) MJ, and (d),(h),(l) JA during (left) the entire period of 1901–2014, and during the (middle) positive and (right) negative AMO phases. The dotted shading shows statistical significance at the 95% confidence level according to the Student's *t* test. The black rectangles in (g) and (k) indicate the Pacific region (40°S–40°N, 120°E–80°W), and the black rectangles in (h) and (l) indicate the North Atlantic region (0°–70°N, 90°W–0°).

with the decaying El Niño, while they are manifested over the North Atlantic (Figs. 4h,l). Considering the great difference in anomalous SST patterns in MJ and JA, we focus on the early and late summer separately to investigate the El Niño–related precipitation anomalies modulated by the AMO in the following section.

b. El Niño–related early summer (MJ) precipitation anomalies modulated by the AMO

Previous studies have pointed out that El Niño influences the East Asian climate via the WNPAC (Wang et al. 2000; Wu et al. 2010; Wu et al. 2017). Different strengths or positions of the WNPAC lead to different influences on the climatological circulation, inducing different anomalous precipitation patterns in SC and the ICP (Gong and Ho 2002; Zhang and Sumi 2002; Chan and Zhou 2005; Zhou et al. 2009; Y. Huang et al. 2015; Matsumura et al. 2015; Ge et al. 2017; Zhang et al. 2017).

In early summer, the El Niño–related SSTAs over the western North Pacific are crucial for the maintenance of the WNPAC (Wang et al. 2000; Wang et al. 2008; Wu et al. 2010; Wu et al. 2014; Wu et al. 2017). Induced by El Niño–related SSTAs, the suppressed convective heating over the western Pacific leads to the formation of WNPAC in the winter of an El Niño mature period (Gill 1980; Wang et al. 2000). Generally, the anomalous cold SSTs in the western North Pacific persist from January to June (Figs. 4a–c) and induce ocean surface cooling and positive air–sea interaction feedback, thus contributing to the maintenance of WNPAC in early summer (Wang et al. 2000). As mentioned above, during positive phases of the AMO, the cold SSTAs in the western North Pacific have disappeared in MJ (Fig. 4g), whereas they are still significant during negative phases (Fig. 4k). As a result, in MJ the El Niño–induced WNPAC is stronger (weaker) than normal during negative (positive) phases of the AMO (Figs. 5a,d,g).

As shown in Fig. 5, the El Niño–related WNPAC is located at approximately 15°N, 140°E (Fig. 5a), and the westerly (easterly) anomalies on the (north) south flank

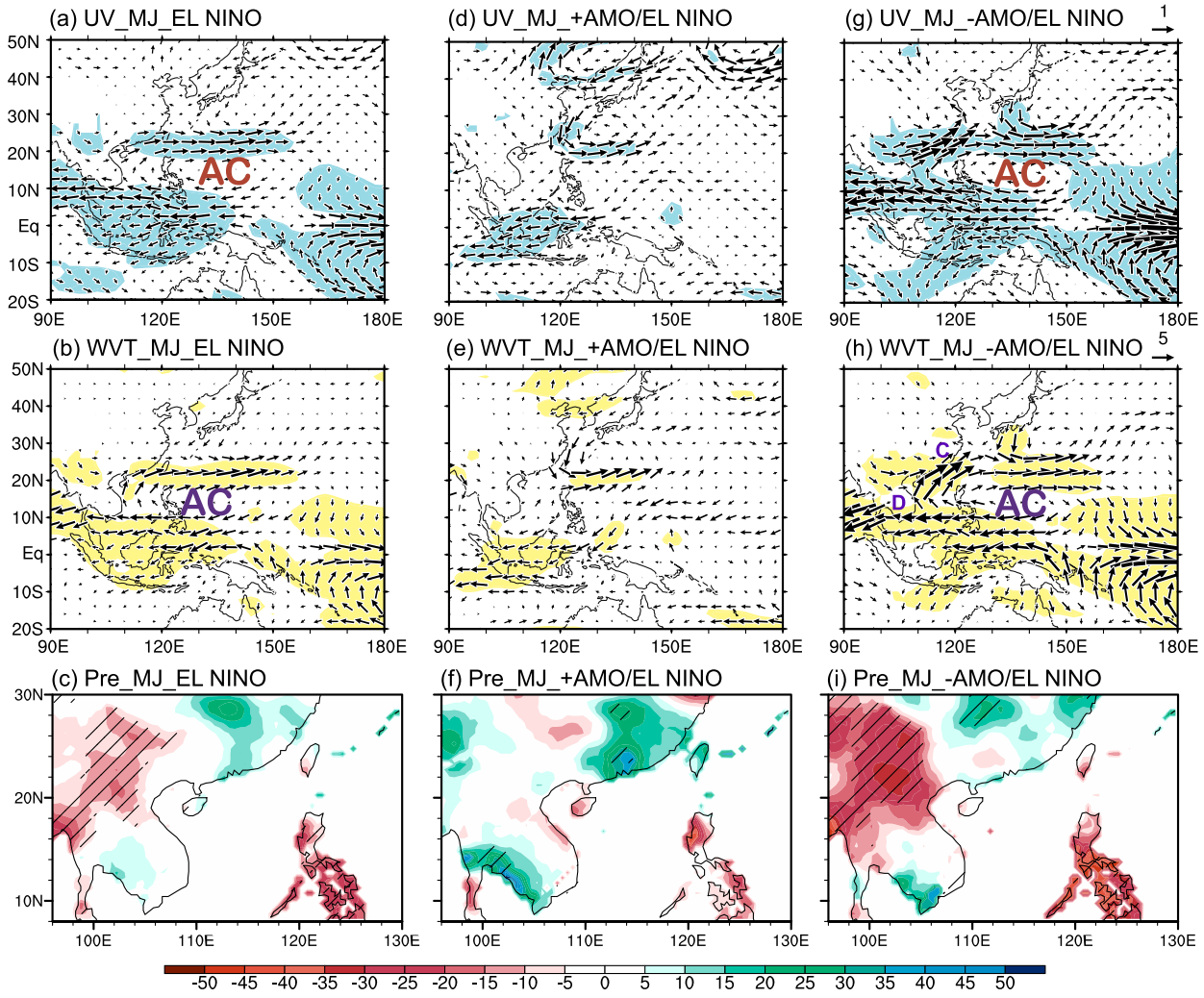

FIG. 5. Anomalous (a),(d),(g) 850-hPa winds (m s^{-1}), (b),(e),(h) vertically integrated water vapor transport (kg m^{-1} s^{-1}), and (c),(f),(i) precipitation derived from the CRU TS4.01 dataset (mm $month^{-1}$) in MJ during (left) the entire period of 1901–2014, (middle) +AMO/El Niño, and (right) −AMO/El Niño. The marker "AC" in (a), (b), (g), and (h) represents an anticyclone. "D" and "C" in (h) represent divergence and convergence, respectively. The shading in (a), (b), (d), (e), (g), and (h) and the hatched shading in (c), (f), and (i) show statistical significance at the 95% confidence level according to the Student's *t* test.

of the WNPAC enhance (reduce) the climatological wind (Fig. 5a) and water vapor transport over SC (the ICP) (Fig. 5b), leading to wet (dry) anomalies (Fig. 5c). During positive phases of the AMO, the El Niño–related WNPAC is weaker than normal (Figs. 5a,d). A cyclonic anomaly is located over the northern portion of the Philippine Sea (Fig. 5d), influencing water vapor transport (Fig. 5e) and precipitation anomalies in southeastern China (Fig. 5f). For the ICP and southwestern China, there are no significant moisture transport anomalies (Fig. 5e) or precipitation anomalies (Fig. 5f; see also Figs. S1a and S2a in the online supplemental material). During negative phases of the AMO, the WNPAC is stronger than normal, and its center is located around 15°N, 140°E (Fig. 5g). Therefore, anomalous southwesterlies (easterlies) on the northwest (southwest) flank of the WNPAC enhance (reduce) the climatological southwesterlies (westerlies) over SC (the ICP) (Fig. 5g), leading to anomalous water vapor convergence (divergence) (Fig. 5h) and significant wet (dry) anomalies (Fig. 5i; see also Figs. S1c and S2c) over SC (the ICP). To sum up: In MJ during the negative phases of AMO, colder than normal western North Pacific favors the maintaining of the WNPAC. Consequently, southerly (westerly) anomalies on the northwest (southwest) flank of the WNPAC enhance (reduce) the moisture transport and precipitation anomalies in SC (the ICP). In contrast, during positive AMO phases,

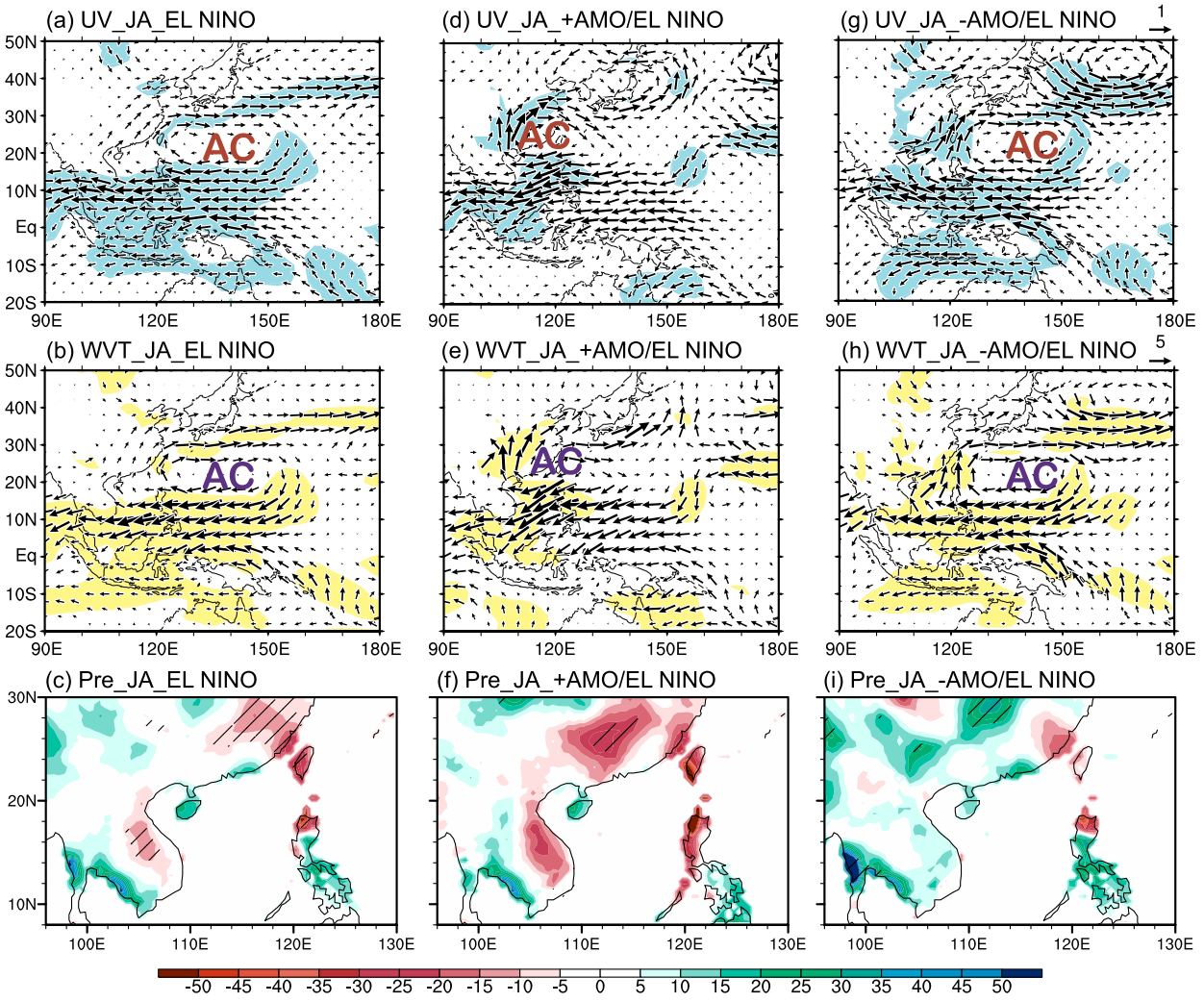

FIG. 6. As in Fig. 5, but for the anomalies in JA.

weak SSTAs over the western North Pacific lead to limited influence on the precipitation in Southeast Asia.

c. *El Niño–related late summer (JA) precipitation anomalies modulated by the AMO*

In late summer, when El Niño decays, although the El Niño–related SSTAs are generally weak in the eastern and central tropical Pacific, El Niño also has an impact on the WNPAC via affecting SSTAs in the western North Pacific and Indian Ocean, as well as the combination mode. The anomalous warming in the Indian Ocean contributes to the WNPAC persistence through excitation of a tropospheric Kelvin wave, suppressing convection over the western North Pacific (Xie et al. 2009). Therefore, the El Niño–related WNPAC still persists in JA (Fig. 6a), exerting effects on the water vapor transport (Fig. 6b) and precipitation (Fig. 6c) in Southeast Asia. During positive phases of the AMO, however, the El Niño–related WNPAC (Fig. 6d) is located around 20°N, 115°E, being westward from the climatological state (Fig. 6a). The strengthened and westward-shifted WNPAC during positive phases of the AMO can be attributed to the AMO modulation of mid- to high-latitude wave activities. [Note that in MJ the anomalous wave activities show insignificant influences on the climate in SC and the ICP during both positive (Fig. S3a) and negative (Fig. S3b) phases of the AMO.] In JA, during positive phases of the AMO, accompanied by warmer than normal SSTAs over the North Atlantic (Fig. 4h), anomalous convergence (divergence) in the lower (upper) troposphere (Fig. S4) provides a vorticity source for generating Rossby waves (Sardeshmukh and Hoskins 1988; Qin and Robinson 1993). The warm SSTAs in the North Atlantic may influence the diabatic heating and transient eddy activities over the North Atlantic, exciting an arching wave train that propagates

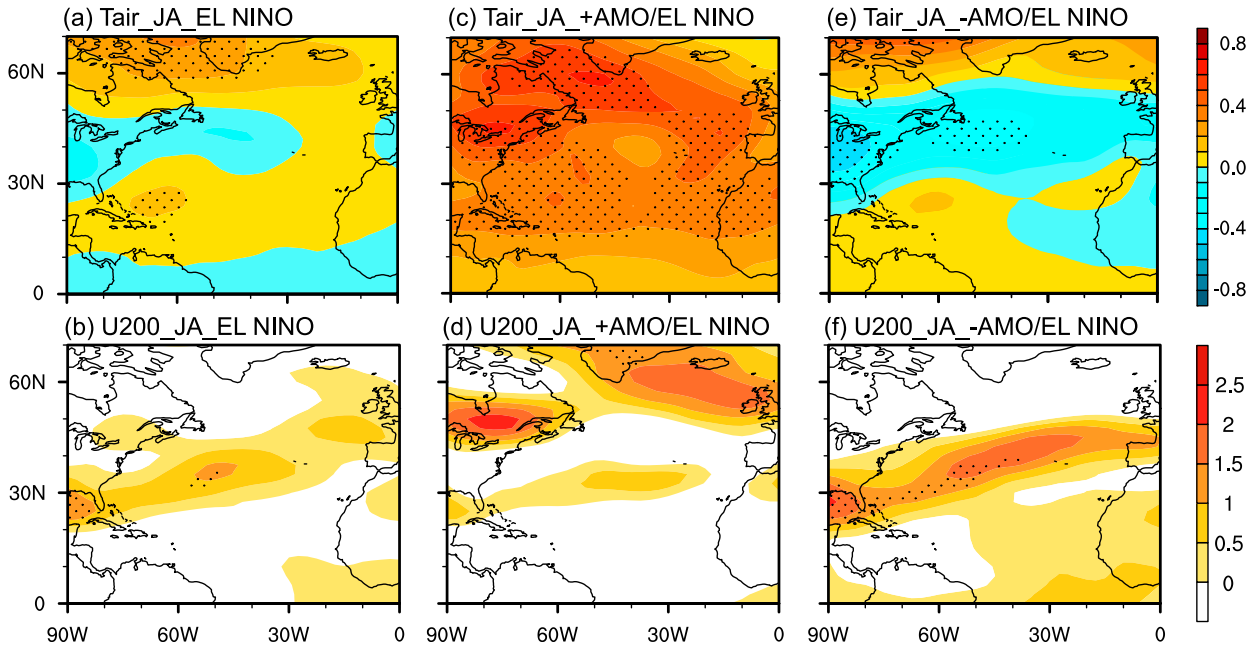

FIG. 7. Anomalous (a),(c),(e) vertically integrated tropospheric temperatures between 200 and 600 hPa (K), and (b),(d),(f) zonal wind speeds ($m\ s^{-1}$) at 200 hPa in JA for the composites of El Niño events during (left) the entire period of 1901–2014 and (middle) +AMO/El Niño and (right) −AMO/El Niño. The dotted shading shows statistical significance at the 95% confidence level according to the Student's *t* test.

along a "great circle route" from the North Atlantic to East Asia (Li et al. 2008; Zhu et al. 2011; Fan et al. 2018). As shown in Fig. 7, compared to the climatological state (Fig. 7a), the anomalous upper-troposphere meridional temperature gradient over the North Atlantic during positive phases of the AMO (Fig. 7c) favors a weaker than normal subtropical westerly jet over the North Atlantic and a stronger than normal and more northward subpolar jet (Figs. 7b,d). As pointed out by Zhu et al. (2011), the large-scale setting during positive AMO phases corresponding to a more northeastward-tilted North Atlantic storm track favors the Scandinavian–Southeast Asia wave train. Additionally, the positive AMO phase is characterized by an increasing frequency of strong positive North Atlantic Oscillation events in summer, which could strengthen the North Atlantic storm tracks, influencing the propagation of anomalous wave activities (Goswami et al. 2006; Rodríguez-Fonseca et al. 2016). Therefore, as shown in Fig. 8, an anomalous wave train originates in the North Atlantic, propagates northeastward to Scandinavia, and then heads southeastward to the Ural Mountains (Fig. 8a), inducing a high pressure anomaly over SC in JA (Fig. 8b) during positive phases of the AMO. As a result, during positive phases of the AMO, SC is mostly under the control of the anomalous anticyclone whereas the ICP is influenced by the easterly anomalies on the southwest flank of the anticyclone (Fig. 6d). Consequently, the anomalous anticyclone weakens the climatological low-level winds, leading to anomalous water vapor divergence (Fig. 6e) and thus dry anomalies (Fig. 6f, Figs. S1b and S2b) in SC and the eastern ICP.

Unlike positive AMO phases, Southeast Asia is less influenced by the anomalous mid- to high-latitude wave activities during negative phases. As shown in Fig. 7, the stronger than normal meridional temperature gradient around 30°N (Figs. 7a,e) tends to strengthen the subtropical Atlantic jet (Figs. 7b,f). As a result, the anomalous wave train over the North Atlantic propagates straight eastward (Fig. 8c), rather than northward to Scandinavia during positive AMO phases (Fig. 8a). Furthermore, the anomalous wave activity propagating from Europe to Northeast Asia along the summer Asian jet acts as a waveguide (Hoskins and Ambrizzi 1993; Schneidereit et al. 2012; Orsolini et al. 2015) and therefore exhibits limited influence on the climate in SC and the ICP (Figs. 8c,d). Consequently, in JA during AMO negative phases, the WNPAC center is located around 20°N, 145°E (Fig. 6g), which is similar to the climatology condition (Fig. 6a), showing weak influences on the climatological low-level winds (Fig. 6g), water vapor transport (Fig. 6h), and the precipitation anomalies (Fig. 6i; see also Figs. S1d and S2d) over SC and the ICP.

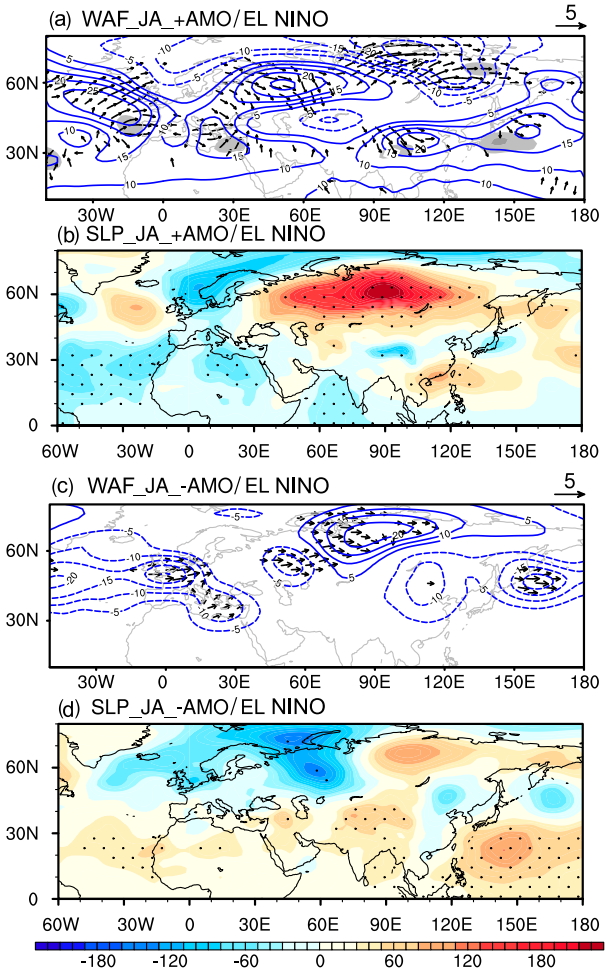

FIG. 8. Anomalous (a),(c) wave activity flux (vectors; $m^2 s^{-2}$) and geopotential height (contours; gpm) at 300 hPa, and (b),(d) sea level pressure (Pa) in JA during +AMO/El Niño in (a) and (b) and −AMO/El Niño in (c) and (d) for the period of 1901–2014. The shading in (a) and (c) and the dotted shading in (b) and (d) show statistical significance at the 95% confidence level according to the Student's *t* test.

d. Model simulation

How well the state-of-art coupled model GFDL CM3 works in simulating the El Niño–related precipitation anomalies during different phases of the AMO is evaluated in this section. Compared with the reanalysis (Fig. 2), GFDL CM3 reasonably represents distributions of climatological wind fields and precipitation in MJ and JA over both SC and the ICP (Fig. 9). With similar methods as those used for the reanalysis data, the El Niño events during positive and negative AMO phases are then determined for composite analysis based on the GFDL CM3 historical simulation during 1901–2005. First, compared with the reanalysis data (Fig. 3), GFDL CM3 captures the characteristics of the climatological warm (cold) SSTAs over the western North Pacific during positive (negative) phases of the AMO (Fig. 10). Additionally, results based on GFDL CM3 also suggest that during positive phases of the AMO, El Niño–related SSTAs over the western North Pacific decay faster (Figs. 11e–g) than those during negative phases of the AMO (Figs. 11i–l). Moreover, the model simulation reproduces the weaker (stronger) than normal WNPAC, water vapor transport, and precipitation anomalies in MJ during positive (negative) phases of the AMO (Fig. 12), which is consistent with the reanalysis results (Fig. 5). It should be noted that, in MJ, the reanalysis results show that the WNPAC is not significant during the positive AMO phases (Fig. 5d), whereas the GFDL CM3 simulation shows a persistent WNPAC (Fig. 12d). The bias could be attributed to differences in the decay speed of the El Niño–related SSTA pattern during positive AMO phases between model simulations (Figs. 11e–g) and the reanalysis (Figs. 4e–g): in MJ, the cold SSTAs over the western North Pacific are not significant in the reanalysis (Fig. 4g), while they are still retained in the model simulation (Fig. 11g). Correspondingly, the simulated circulation anomaly (Fig. 12d) is stronger compared to that of the reanalysis (Fig. 5d).

In JA, the circulation, water vapor transport, and precipitation anomalies during positive AMO phases derived from the GFDL CM3 simulation (Figs. 13d–f) show similar characteristics with the reanalysis (Figs. 6d–f). However, the simulated WNPAC during negative phases of the AMO shifts more westward (Fig. 13g) than the reanalysis (Fig. 6g), leading to biases for simulated water vapor transport (Fig. 13h) and precipitation anomalies (Fig. 13i). Namely, significant dry (wet) anomalies occur over SC (the ICP) (Fig. 13i), which is inconsistent with the reanalysis (Fig. 6i). In addition, during positive phases of the AMO, the model simulation can hardly reproduce the anomalous wave activity propagation (Fig. S5). The simulated WNPAC is shifted northward (Fig. 13d) relative to the reanalysis (Fig. 6d). To sum up, the GFDL CM3 simulation shows a certain consistency with the reanalysis, with biases mainly due to its limited ability in simulating the mid- to high-latitude processes.

4. Summary and discussion

El Niño–related summer precipitation anomalies in SC and the ICP show different bimonthly variations during different phases of the AMO.

(i) In MJ, the AMO affects the tropical air–sea interaction via modulating the western North Pacific SSTs and the strength of ENSO, further influencing

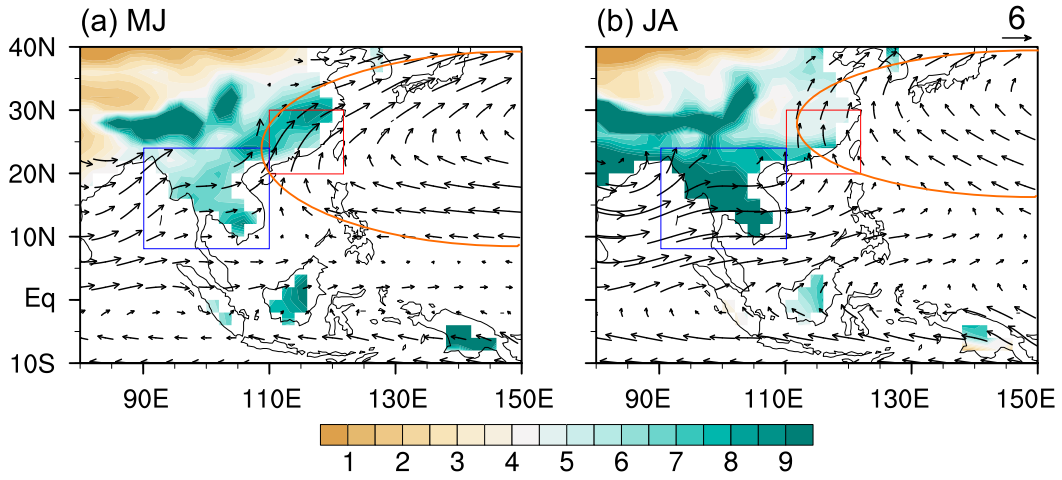

FIG. 9. As in Fig. 2, but with the results derived from GFDL CM3 for the period of 1901–2005 (shadings; mm day^{-1}).

the intensity and position of the El Niño–related WNPAC and leading to anomalous precipitation in SC and the ICP. Results show that El Niño and the corresponding SSTAs are stronger and persist longer during negative phases of the AMO than during positive phases (Fig. 4). In MJ during positive phases of the AMO, the relatively weak SSTAs over the western North Pacific (Fig. 4g) lead to a short persistence of the WNPAC, with limited influence on the precipitation anomalies over SC and the ICP (Figs. 5d–f). By contrast, during negative phases of the AMO, the El Niño–related cold SSTAs (Fig. 4k)

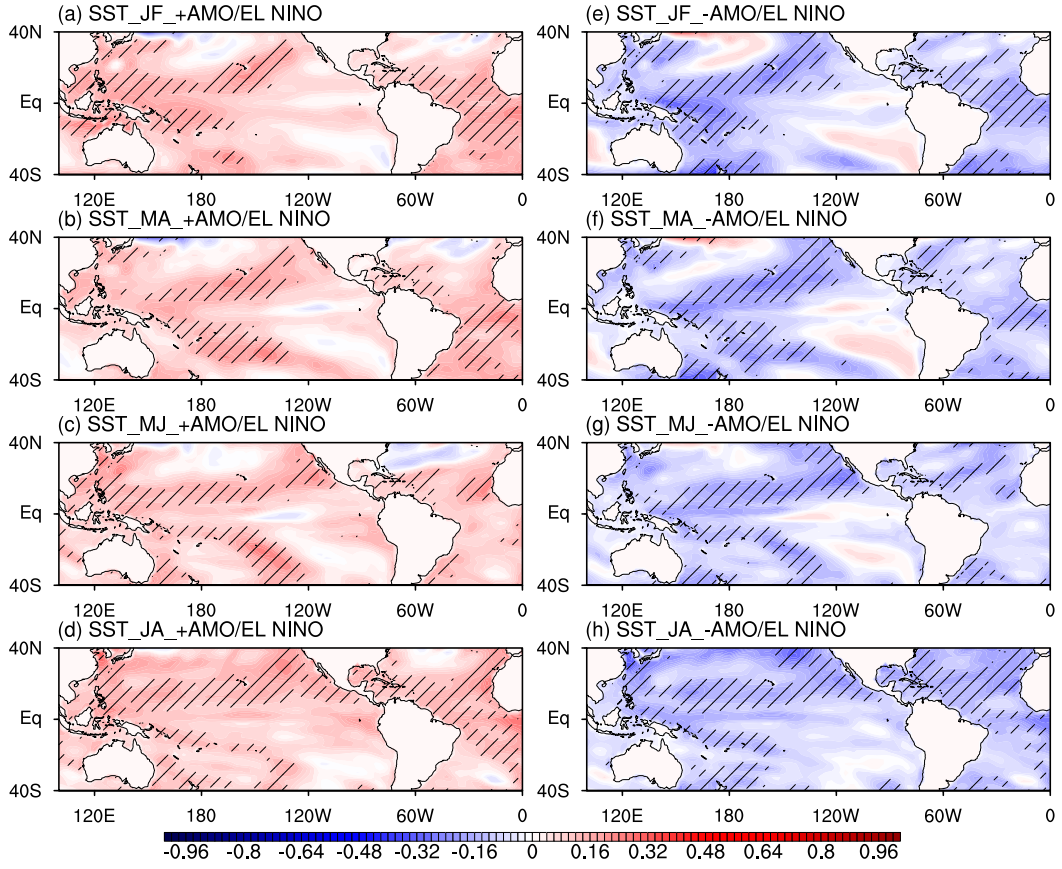

FIG. 10. As in Fig. 3, but with the results derived from GFDL CM3 for the period of 1901–2005.

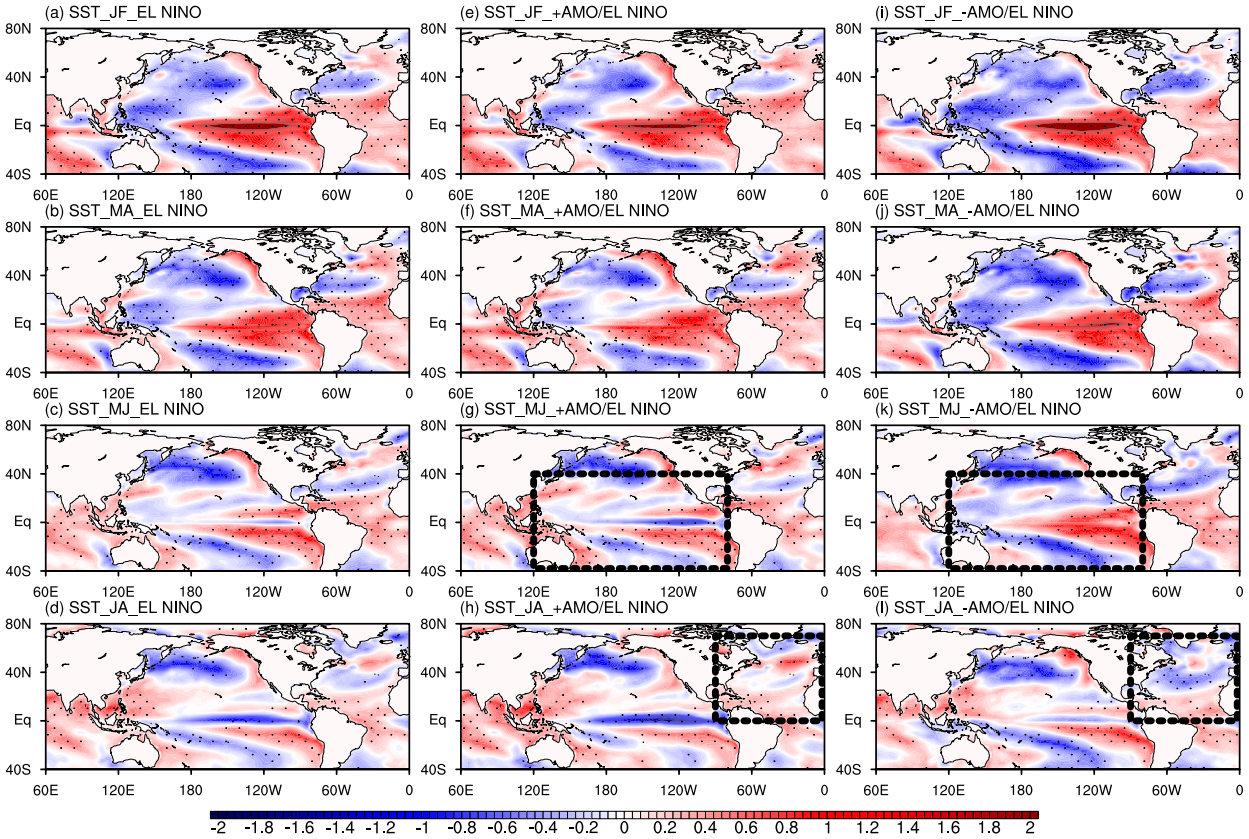

FIG. 11. As in Fig. 4, but with the results derived from GFDL CM3 for the period of 1901–2005.

over the western North Pacific favor persistence of the WNPAC (Fig. 5g). Therefore, the anomalous southwesterlies (easterlies) on the northwest (southwest) flank of the WNPAC strengthen (weaken) the monsoon flow over SC (the ICP), leading to wet (dry) anomalies (Figs. 5g–i). In conclusion, during positive phases of the AMO, the weak El Niño–related SSTAs have a limited influence on the monsoon flow. During negative phases of the AMO, maintained by the El Niño–related cold SSTAs over the western North Pacific, the WNPAC modifies the climatological wind, leading to wet and dry anomalies in SC and the ICP, respectively.

(ii) In JA, SSTAs in the tropical Pacific weaken with El Niño decaying, manifesting the teleconnection impact from the North Atlantic. During positive phases of the AMO, the subtropical jet is weaker than normal, and the subpolar jet over the North Atlantic shifts northward (Figs. 7b,d). The warm SSTAs in the North Atlantic (Fig. 4h) impact the diabatic heating and transient eddy activities over the North Atlantic (Li et al. 2008; Zhu et al. 2011). Therefore, during positive phases of the AMO, anomalous wave train tends to propagate along a ''great circle route'' from the North Atlantic to East Asia (Fig. 8a), inducing a high pressure anomaly over SC and the ICP (Fig. 8b), accompanied by negative precipitation anomalies (Fig. 6f). During negative phases of the AMO, cold SSTAs in the North Atlantic enhance the meridional temperature gradient over 30°N (Fig. 7e). Correspondingly, the subtropical Atlantic jet strengthens and is more zonally oriented (Fig. 7f) compared to the climatological composite of all El Niño events (Fig. 7b). With these large-scale conditions, the anomalous wave train tends to propagate eastward (Fig. 8c) rather than northward to Scandinavia during positive AMO phases (Fig. 8a), showing limited influences on the precipitation in SC and the ICP (Fig. 6i). In summary, during positive phases of the AMO, the North Atlantic is warmer than normal, and the subpolar jet shifts northward. The anomalous wave train tends to propagate along a great circle route and leads to dry anomalies in SC and the ICP. During negative phases of the AMO, the colder North Atlantic and warmer tropical Atlantic favor a more zonally oriented subtropical jet, and the anomalous wave train propagates straightly eastward, with limited influence on SC and the ICP.

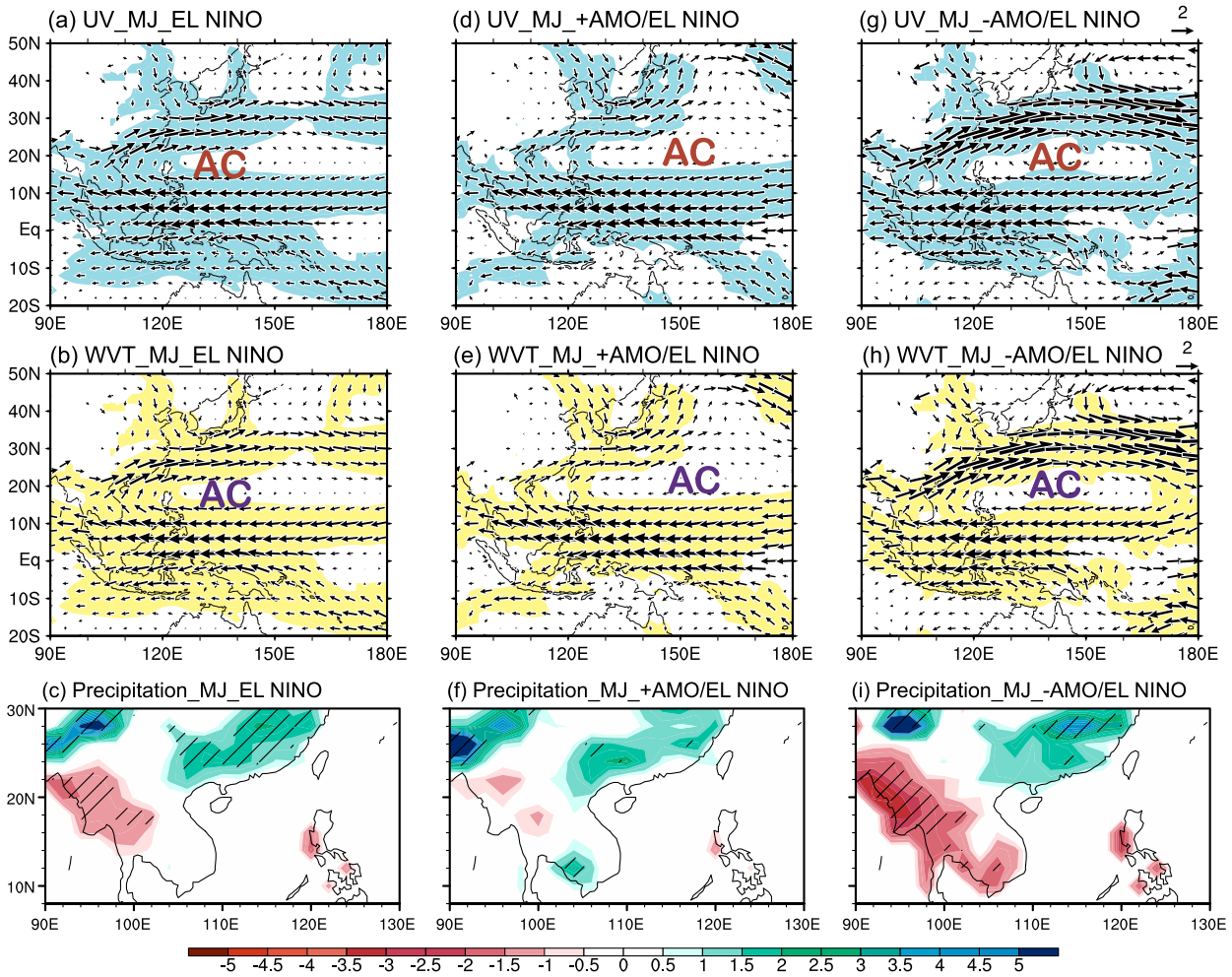

FIG. 12. As in Fig. 5, but with the results derived from GFDL CM3 for the period of 1901–2005.

Additionally, we evaluated the GFDL CM3 on simulating the abovementioned mechanisms. It is concluded that, in MJ of an El Niño decaying year, the model reasonably reproduces the slowly (fast) decaying SSTAs (Fig. 11), a strong (weak) WNPAC, and strong (weak) water vapor transport and precipitation anomalies in Southeast Asia during negative (positive) phases of the AMO (Fig. 12). In JA of an El Niño decaying year, model simulations are characterized by large biases in the mid- to high-latitude wave activity anomalies (Fig. S5) compared with the reanalysis (Fig. 8). Therefore, the associated circulation and precipitation anomalies are unsatisfactorily represented. Besides, analyses of the other CMIP5 models indicate that CCSM4 and FIO-ESM, which are provided respectively by the National Center for Atmospheric Research (NCAR) and the First Institute of Oceanography, State Oceanic Administration of China, also reasonably generate the WNPAC and anomalous water vapor transport but fail to reproduce the wave activity anomalies in JA (figures not shown). Biases of model simulations could be attributed to the following factors. First, the simulated western North Pacific subtropical high in the CMIP5 model is westward from the observations in most cases (He and Zhou 2014). Second, large uncertainties always feature the model simulations on climate internal variability and nonlinear progresses. The evaluations indicate that the used models show limited ability in reproducing the mid- to high-latitude processes, suggesting the great importance of further improvement in simulations on mid- to high-latitude processes.

Our study illustrates the role that the AMO plays in modulating the El Niño–related summer precipitation anomalies in SC and the ICP. However, it should be noted that it is difficult to detect a causal relationship based on statistical methods. In addition, there are still many other factors that impact the El Niño–precipitation

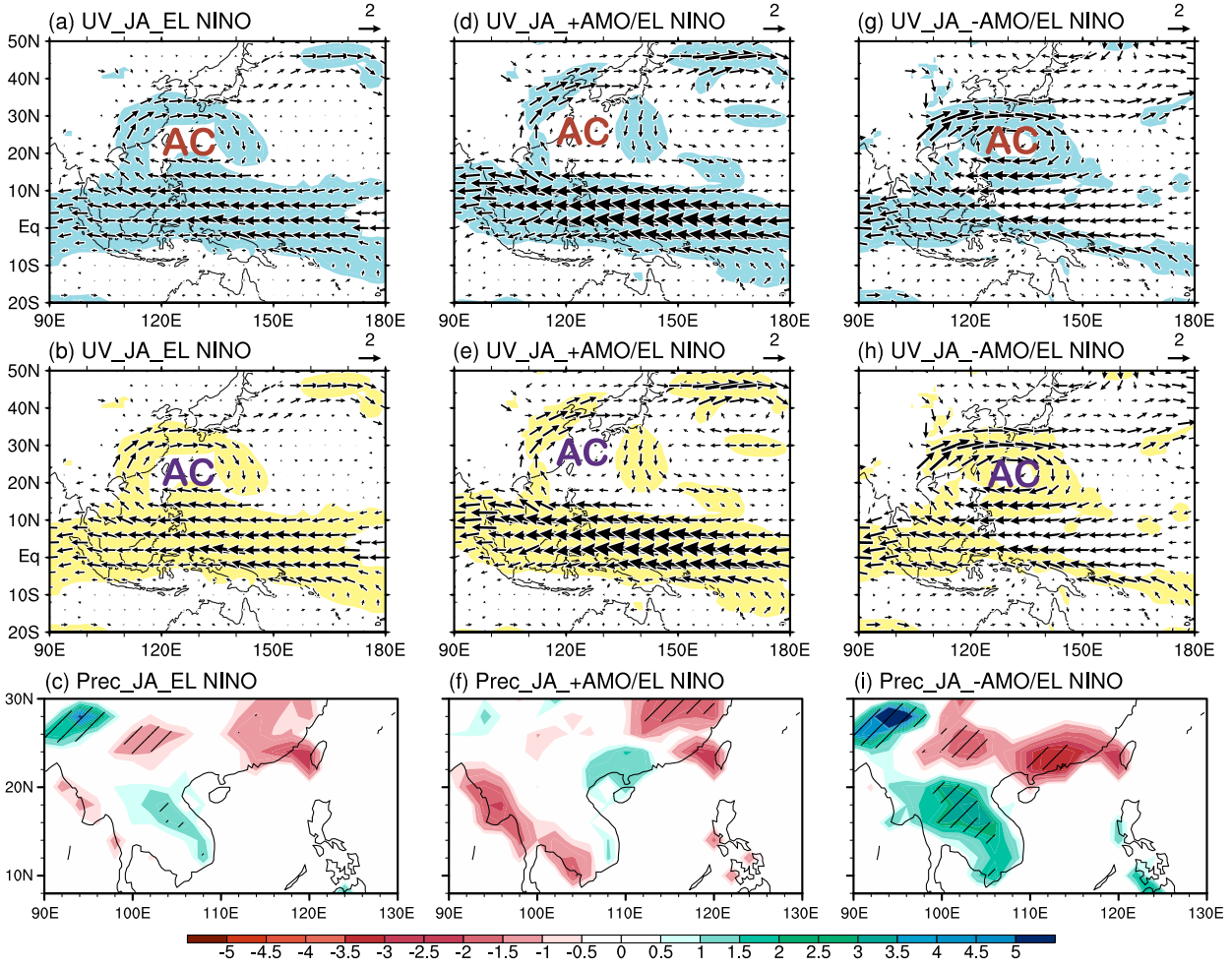

FIG. 13. As in Fig. 6, but with the results derived from GFDL CM3 for the period of 1901–2005.

relationship, such as the Pacific decadal oscillation and the Indian Ocean SSTs (Chan and Zhou 2005; Wu and Mao 2016; Chen et al. 2018). Further investigation into the relative importance and the specific influence of these factors is needed to provide a deeper understanding of the El Niño–precipitation relationship. Moreover, the diversity of El Niño events has not yet been considered in this study. Since the impacts of the central Pacific El Niño are different from those of the eastern Pacific El Niño, it is also necessary to take El Niño types into consideration in further investigations.

Acknowledgments. This research was jointly supported by the National Key R&D Program of China (Grant 2017YFA0603802), the National Natural Science Foundation of China (Grants 41730964 and 41421004), and the China Scholarship Council (Grant 201704910621). We thank the three anonymous reviewers for their insightful comments and suggestions. We thank Dr. Zhiqing Xu for very helpful discussions and the German Climate Computing Center (DKRZ) for providing computing resources.

REFERENCES

Cai, W., and Coauthors, 2014: Increasing frequency of extreme El Niño events due to greenhouse warming. *Nat. Climate Change*, **4**, 111–116, https://doi.org/10.1038/nclimate2100.

Chan, J. C. L., and W. Zhou, 2005: PDO, ENSO and the early summer monsoon rainfall over South China. *Geophys. Res. Lett.*, **32**, L08810, https://doi.org/10.1029/2004GL022015.

Chen, J., Z. Wen, R. Wu, Z. Chen, and P. Zhao, 2014: Interdecadal changes in the relationship between southern China winter–spring precipitation and El Niño. *Climate Dyn.*, **43**, 1327–1338, https://doi.org/10.1007/s00382-013-1947-x.

——, X. Wang, W. Zhou, C. Wang, Q. Xie, G. Li, and S. Chen, 2018: Unusual rainfall in southern China in decaying August during extreme El Niño 2015/16: Role of the western Indian Ocean and north tropical Atlantic SST. *J. Climate*, **31**, 7019–7034, https://doi.org/10.1175/JCLI-D-17-0827.1.

Compo, G. P., J. S. Whitaker, and P. D. Sardeshmukh, 2006: Feasibility of a 100-yr reanalysis using only surface pressure data. *Bull. Amer. Meteor. Soc.*, **87**, 175–190, https://doi.org/10.1175/BAMS-87-2-175.

Dai, A., and T. M. L. Wigley, 2000: Global patterns of ENSO-induced precipitation. *Geophys. Res. Lett.*, **27**, 1283–1286, https://doi.org/10.1029/1999GL011140.

Ding, Y., and G. Hu, 2003: A study on water vapor budget over China during the 1998 severe flood periods (in Chinese). *Acta Meteor. Sin.*, **61**, 129–145.

Dong, B., R. T. Sutton, and A. A. Scaife, 2006: Multidecadal modulation of El Niño–Southern Oscillation (ENSO) variance by Atlantic Ocean sea surface temperatures. *Geophys. Res. Lett.*, **33**, L08705, https://doi.org/10.1029/2006GL025766.

Enfield, D. B., A. M. Mestas-Nuñez, and P. J. Trimble, 2001: The Atlantic Multidecadal Oscillation and its relationship to rainfall and river flows in the continental U.S. *Geophys. Res. Lett.*, **28**, 2077–2080, https://doi.org/10.1029/2000GL012745.

Fan, Y., K. Fan, Z. Xu, and S. Li, 2018: ENSO–South China Sea summer monsoon interaction modulated by the Atlantic multidecadal oscillation. *J. Climate*, **31**, 3061–3076, https://doi.org/10.1175/JCLI-D-17-0448.1.

Ge, F., X. Zhi, Z. A. Babar, W. Tang, and P. Chen, 2017: Interannual variability of summer monsoon precipitation over the Indochina Peninsula in association with ENSO. *Theor. Appl. Climatol.*, **128**, 523–531, https://doi.org/10.1007/s00704-015-1729-y.

Geng, X., W. Zhang, M. F. Stuecker, P. Liu, F.-F. Jin, and G. Tan, 2017: Decadal modulation of the ENSO–East Asian winter monsoon relationship by the Atlantic multidecadal oscillation. *Climate Dyn.*, **49**, 2531–2544, https://doi.org/10.1007/s00382-016-3465-0.

——, ——, F.-F. Jin, and M. F. Stuecker, 2018: A new method for interpreting nonstationary running correlations and its application to the ENSO–EAWM relationship. *Geophys. Res. Lett.*, **45**, 327–334, https://doi.org/10.1002/2017GL076564.

Gill, A. E., 1980: Some simple solutions for heat-induced tropical circulation. *Quart. J. Roy. Meteor. Soc.*, **106**, 447–462, https://doi.org/10.1002/qj.49710644905.

Gill, E. C., B. Rajagopalan, and P. Molnar, 2015: Subseasonal variations in spatial signatures of ENSO on the Indian summer monsoon from 1901 to 2009. *J. Geophys. Res.*, **120**, 8165–8185, https://doi.org/10.1002/2015JD023184.

Goly, A., and R. S. V. Teegavarapu, 2014: Individual and coupled influences of AMO and ENSO on regional precipitation characteristics and extremes. *Water Resour. Res.*, **50**, 4686–4709, https://doi.org/10.1002/2013WR014540.

Gong, D., and C. Ho, 2002: Shift in the summer rainfall over the Yangtze River valley in the late 1970s. *Geophys. Res. Lett.*, **29**, 1436, https://doi.org/10.1029/2001GL014523.

Goswami, B. N., M. S. Madhusoodanan, C. P. Neema, and D. Sengupta, 2006: A physical mechanism for North Atlantic SST influence on the Indian summer monsoon. *Geophys. Res. Lett.*, **33**, L02706, https://doi.org/10.1029/2005GL024803.

Griffies, S. M., and Coauthors, 2011: The GFDL CM3 coupled climate model: Characteristics of the ocean and sea ice simulations. *J. Climate*, **24**, 3520–3544, https://doi.org/10.1175/2011JCLI3964.1.

Hao, X., and S. He, 2017: Combined effect of ENSO-like and Atlantic multidecadal oscillation SSTAs on the interannual variability of the East Asian winter monsoon. *J. Climate*, **30**, 2697–2716, https://doi.org/10.1175/JCLI-D-16-0118.1.

He, C., and T. Zhou, 2014: The two interannual variability modes of the western North Pacific subtropical high simulated by 28 CMIP5–AMIP models. *Climate Dyn.*, **43**, 2455–2469, https://doi.org/10.1007/s00382-014-2068-x.

Hoskins, B. J., and T. Ambrizzi, 1993: Rossby wave propagation on a realistic longitudinally varying flow. *J. Atmos. Sci.*, **50**, 1661–1671, https://doi.org/10.1175/1520-0469(1993)050<1661:RWPOAR>2.0.CO;2.

Hu, Q., and S. Feng, 2012: AMO- and ENSO-driven summertime circulation and precipitation variations in North America. *J. Climate*, **25**, 6477–6495, https://doi.org/10.1175/JCLI-D-11-00520.1.

Huang, B., and Coauthors, 2015: Extended reconstructed sea surface temperature version 4 (ERSST.v4). Part I: Upgrades and intercomparisons. *J. Climate*, **28**, 911–930, https://doi.org/10.1175/JCLI-D-14-00006.1.

Huang, R., and Y. Wu, 1989: The influence of ENSO on the summer climate change in China and its mechanism. *Adv. Atmos. Sci.*, **6**, 21–32, https://doi.org/10.1007/BF02656915.

Huang, Y., H. Wang, K. Fan, and Y. Gao, 2015: The western Pacific subtropical high after the 1970s: Westward or eastward shift? *Climate Dyn.*, **44**, 2035–2047, https://doi.org/10.1007/s00382-014-2194-5.

Jung, E., and B. P. Kirtman, 2016: ENSO modulation of tropical Indian Ocean subseasonal variability. *Geophys. Res. Lett.*, **43**, 12 634–12 642, https://doi.org/10.1002/2016GL071899.

Kavvada, A., A. Ruiz-Barradas, and S. Nigam, 2013: AMO's structure and climate footprint in observations and IPCC AR5 climate simulations. *Climate Dyn.*, **41**, 1345–1364, https://doi.org/10.1007/s00382-013-1712-1.

Kayano, M. T., and V. B. Capistrano, 2014: How the Atlantic multidecadal oscillation (AMO) modifies the ENSO influence on the South American rainfall. *Int. J. Climatol.*, **34**, 162–178, https://doi.org/10.1002/joc.3674.

Kerr, R. A., 2000: A North Atlantic climate pacemaker for the centuries. *Science*, **288**, 1984–1985, https://doi.org/10.1126/science.288.5473.1984.

Kucharski, F., and Coauthors, 2016: Atlantic forcing of Pacific decadal variability. *Climate Dyn.*, **46**, 2337–2351, https://doi.org/10.1007/s00382-015-2705-z.

Li, C., W. Chen, X. Hong, and R. Lu, 2017: Why was the strengthening of rainfall in summer over the Yangtze River valley in 2016 less pronounced than that in 1998 under similar preceding El Niño events?—Role of midlatitude circulation in August. *Adv. Atmos. Sci.*, **34**, 1290–1300, https://doi.org/10.1007/s00376-017-7003-8.

Li, S., and G. Bates, 2007: Influence of the Atlantic multidecadal oscillation on the winter climate of East China. *Adv. Atmos. Sci.*, **24**, 126–135, https://doi.org/10.1007/s00376-007-0126-6.

——, J. Perlwitz, X. Quan, and M. P. Hoerling, 2008: Modelling the influence of North Atlantic multidecadal warmth on the Indian summer rainfall. *Geophys. Res. Lett.*, **35**, L05804, https://doi.org/10.1029/2007GL032901.

Li, T., B. Wang, B. Wu, T. Zhou, C.-P. Chang, and R. Zhang, 2017: Theories on formation of an anomalous anticyclone in western North Pacific during El Niño: A review. *J. Meteor. Res.*, **31**, 987–1006, https://doi.org/10.1007/s13351-017-7147-6.

Lim, Y. K., and K. Y. Kim, 2007: ENSO impact on the space–time evolution of the regional Asian summer monsoons. *J. Climate*, **20**, 2397–2415, https://doi.org/10.1175/JCLI4120.1.

Lin, L., C. Chen, and M. Luo, 2018: 2018: Impacts of El Niño–Southern Oscillation on heat waves in the Indochina peninsula. *Atmos. Sci. Lett.*, **19**, e856, https://doi.org/10.1002/asl.856.

Lu, R., B. Dong, and D. Hui, 2006: Impact of the Atlantic Multidecadal Oscillation on the Asian summer monsoon. *Geophys. Res. Lett.*, **33**, L24701, https://doi.org/10.1029/2006GL027655.

——, W. Chen, and B. Dong, 2008: How does a weakened Atlantic thermohaline circulation lead to an intensification of the ENSO–South Asian summer monsoon interaction? *Geophys. Res. Lett.*, **35**, L08706, https://doi.org/10.1029/2008GL033394.

Luo, F., S. Li, and T. Furevik, 2011: 2011: The connection between the Atlantic multidecadal oscillation and the Indian summer monsoon in Bergen Climate Model version 2.0. *J. Geophys. Res.*, **116**, D19117, https://doi.org/10.1029/2011JD015848.

Matsumura, S., S. Sugimoto, and T. Sato, 2015: Recent intensification of the western Pacific subtropical high associated with the East Asian summer monsoon. *J. Climate*, **28**, 2873–2883, https://doi.org/10.1175/JCLI-D-14-00569.1.

Nguyen, T. D., C. Uvo, and D. Rosbjerg, 2007: Relationship between the tropical Pacific and Indian Ocean sea-surface temperature and monthly precipitation over the central highlands, Vietnam. *Int. J. Climatol.*, **27**, 1439–1454, https://doi.org/10.1002/joc.1486.

Orsolini, Y. J., L. Zhang, D. H. W. Peters, K. Fraedrich, X. Zhu, A. Schneidereit, and B. van den Hurk, 2015: Extreme precipitation events over north China in August 2010 and their link to eastward-propagating wave-trains across Eurasia: Observations and monthly forecasting. *Quart. J. Roy. Meteor. Soc.*, **141**, 3097–3105, https://doi.org/10.1002/qj.2594.

Qin, J., and W. A. Robinson, 1993: On the Rossby wave source and the steady linear response to tropical forcing. *J. Atmos. Sci.*, **50**, 1819–1823, https://doi.org/10.1175/1520-0469(1993)050<1819:OTRWSA>2.0.CO;2.

Rodríguez-Fonseca, B., and Coauthors, 2016: A review of ENSO influence on the North Atlantic: A non-stationary signal. *Atmosphere*, **7**, 87, https://doi.org/10.3390/atmos7070087.

Ruiz-Barradas, A., S. Nigam, and A. Kavvada, 2013: The Atlantic Multidecadal Oscillation in twentieth century climate simulations: Uneven progress from CMIP3 to CMIP5. *Climate Dyn.*, **41**, 3301–3315, https://doi.org/10.1007/s00382-013-1810-0.

Sardeshmukh, P. D., and B. J. Hoskins, 1988: The generation of global rotational flow by steady idealized tropical divergence. *J. Atmos. Sci.*, **45**, 1228–1251, https://doi.org/10.1175/1520-0469(1988)045<1228:TGOGRF>2.0.CO;2.

Schneidereit, A., S. Schubert, P. Vargin, F. Lunkeit, X. Zhu, D. H. W. Peters, and K. Fraedrich, 2012: Large-scale flow and the long-lasting blocking high over Russia: Summer 2010. *Mon. Wea. Rev.*, **140**, 2967–2981, https://doi.org/10.1175/MWR-D-11-00249.1.

Stuecker, M., F. Jin, A. Timmermann, and S. McGregor, 2015: Combination mode dynamics of the anomalous northwest Pacific anticyclone. *J. Climate*, **28**, 1093–1111, https://doi.org/10.1175/JCLI-D-14-00225.1.

Sun, C., F. Kucharski, J. Li, F. Jin, I. Kang, and R. Ding, 2017: Western tropical Pacific multidecadal variability forced by the Atlantic multidecadal oscillation. *Nat. Commun.*, **8**, 15998, https://doi.org/10.1038/ncomms15998.

Takaya, K., and H. Nakamura, 2001: A formulation of a phase-independent wave-activity flux for stationary and migratory quasigeostrophic eddies on a zonally varying basic flow. *J. Atmos. Sci.*, **58**, 608–627, https://doi.org/10.1175/1520-0469(2001)058<0608:AFOAPI>2.0.CO;2.

Taylor, K. E., R. J. Stouffer, and G. A. Meehl, 2012: An overview of CMIP5 and the experiment design. *Bull. Amer. Meteor. Soc.*, **93**, 485–498, https://doi.org/10.1175/BAMS-D-11-00094.1.

Wang, B., R. Wu, and X. Fu, 2000: Pacific–East Asian teleconnection: How does ENSO affect East Asian climate? *J. Climate*, **13**, 1517–1536, https://doi.org/10.1175/1520-0442(2000)013<1517:PEATHD>2.0.CO;2.

——, T. Zhou, and J. Yang, 2008: Interdecadal changes in the major modes of Asian-Australian monsoon variability: Strengthening relationship with ENSO since the late 1970s. *J. Climate*, **21**, 1771–1789, https://doi.org/10.1175/2007JCLI1981.1.

——, J. Liu, J. Yang, T. Zhou, and Z. Wu, 2009: Distinct principal modes of early and late summer rainfall anomalies in East Asia. *J. Climate*, **22**, 3864–3875, https://doi.org/10.1175/2009JCLI2850.1.

Wang, H., S. He, and J. Liu, 2013: 2013: Present and future relationship between the East Asian winter monsoon and ENSO: Results of CMIP5. *J. Geophys. Res. Oceans*, **118**, 5222–5237, https://doi.org/10.1002/jgrc.20332.

Wang, Q., S. Li, J. Fu, and G. Li, 2012: Formation of the anomalous summer precipitation in east China in 2010 and 1998: A comparison of the impacts of two kinds of El Niño. *Acta Meteor. Sin.*, **26**, 665–682, https://doi.org/10.1007/s13351-012-0601-6.

Wang, Y., S. Li, and D. Luo, 2009: Seasonal response of Asian monsoonal climate to the Atlantic multidecadal oscillation. *J. Geophys. Res.*, **114**, D02112, https://doi.org/10.1029/2008JD010929.

Wu, B., T. Li, and T. Zhou, 2010: Relative contributions of the Indian Ocean and local SST anomalies to the maintenance of the western North Pacific anomalous anticyclone during the El Niño decaying summer. *J. Climate*, **23**, 2974–2986, https://doi.org/10.1175/2010JCLI3300.1.

——, T. Zhou, and T. Li, 2017: Atmospheric dynamic and thermodynamic processes driving the western North Pacific anomalous anticyclone during El Niño. Part I: Maintenance mechanisms. *J. Climate*, **30**, 9621–9635, https://doi.org/10.1175/JCLI-D-16-0489.1.

Wu, J., and X. Gao, 2013: A gridded daily observation dataset over China region and comparison with the other datasets (in Chinese). *Chin. J. Geophys.*, **56**, 1102–1111, https://doi.org/10.6038/CJG20130406.

Wu, R., G. Huang, Z. Du, and K. Hu, 2014: Cross-season relation of the South China Sea precipitation variability between winter and summer. *Climate Dyn.*, **43**, 193–207, https://doi.org/10.1007/s00382-013-1820-y.

Wu, X., and J. Mao, 2016: Interdecadal modulation of ENSO-related spring rainfall over South China by the Pacific Decadal Oscillation. *Climate Dyn.*, **47**, 3203–3220, https://doi.org/10.1007/s00382-016-3021-y.

Xie, S.-P., K. Hu, J. Hafner, H. Tokinaga, Y. Du, G. Huang, and T. Sampe, 2009: Indian Ocean capacitor effect on Indo-western Pacific climate during the summer following El Niño. *J. Climate*, **22**, 730–747, https://doi.org/10.1175/2008JCLI2544.1.

Xing, W., B. Wang, S.-Y. Yim, and K.-J. Ha, 2017: Predictable patterns of the May–June rainfall anomaly over East Asia. *J. Geophys. Res.*, **122**, 2203–2217, https://doi.org/10.1002/2016JD025856.

Yun, K. S., K. H. Seo, and K. J. Ha, 2010: Interdecadal change in the relationship between ENSO and the intraseasonal oscillation in East Asia. *J. Climate*, **23**, 3599–3612, https://doi.org/10.1175/2010JCLI3431.1.

Zhang, L., K. Fraedrich, X. Zhu, F. Sielmann, and X. Zhi, 2015: Interannual variability of winter precipitation in Southeast

China. *Theor. Appl. Climatol.*, **119**, 229–238, https://doi.org/10.1007/s00704-014-1111-5.

Zhang, R., and T. L. Delworth, 2005: Simulated tropical response to a substantial weakening of the Atlantic thermohaline circulation. *J. Climate*, **18**, 1853–1860, https://doi.org/10.1175/JCLI3460.1.

——, and ——, 2007: Impact of the Atlantic multidecadal oscillation on North Pacific climate variability. *Geophys. Res. Lett.*, **34**, L23708, https://doi.org/10.1029/2007GL031601.

Zhang, R. H., and A. Sumi, 2002: Moisture circulation over East Asia during El Niño episode in northern winter, spring and autumn. *J. Meteor. Soc. Japan*, **80**, 213–227, https://doi.org/10.2151/jmsj.80.213.

——, ——, and M. Kimoto, 1999: A diagnostic study of the impact of El Niño on the precipitation in China. *Adv. Atmos. Sci.*, **16**, 229–241, https://doi.org/10.1007/BF02973084.

——, Q. Min, and J. Su, 2017: Impact of El Niño on atmospheric circulations over East Asia and rainfall in China: Role of the anomalous western North Pacific anticyclone. *Sci. China Earth Sci.*, **60**, 1124–1132, https://doi.org/10.1007/s11430-016-9026-x.

Zhang, W., and Coauthors, 2016: Unraveling El Niño's impact on the East Asian monsoon and Yangtze River summer flooding. *Geophys. Res. Lett.*, **43**, 11 375–11 382, https://doi.org/10.1002/2016GL071190.

Zhang, Y., B. Li, and D. Zheng, 2002: A discussion on the boundary and area of the Tibetan Plateau in China. *Geogr. Res.*, **21**, 1–8, https://doi.org/10.11821/YJ2002010001.

Zhou, T., and Coauthors, 2009: Why the western Pacific subtropical high has extended westward since the late 1970s. *J. Climate*, **22**, 2199–2215, https://doi.org/10.1175/2008JCLI2527.1.

Zhu, X., O. Bothe, and K. Fraedrich, 2011: Summer atmospheric bridging between Europe and East Asia: Influences on drought and wetness on the Tibetan Plateau. *Quat. Int.*, **236**, 151–157, https://doi.org/10.1016/j.quaint.2010.06.015.